Robblee, J.H., Messinger, J., Cinco, R.M., McFarlane, K.L., Fernandez, C., Pizarro, S.A., Sauer, K., Yachandra, V.K.

The Mn cluster in the S_0 state of the oxygen-evolving complex of photosystem II studied by EXAFS spectroscopy: Are there three di-μ-oxo bridged Mn_2 moieties in the tetranuclear Mn complex?

Journal of the American Chemical Society

Supporting Information

Additional XAS experimental details

The synchrotron ring SPEAR was operated at 3.0 GeV at 50 – 100 mA beam current. Energy resolution of the unfocused incoming X-rays was achieved using a Si(220) double-crystal monochromator, which was detuned to 50 % of maximal flux to attenuate harmonic X-rays. A N_2-filled ion chamber (I_0) was mounted in front of the sample to monitor incident beam intensity. An incident X-ray beam of 1.4 mm x 11 mm dimensions with a flux of approximately 3.5 x 10^{10} photons/sec was used for the EXAFS experiments; the total photon flux on the sample was 1.6 x 10^9 photons/sec/mm^2 of sample. The samples were placed at an angle of 45° relative to the X-ray beam and were kept at 10 ± 1 K in a He atmosphere at ambient pressure using an Oxford CF-1208 continuous-flow liquid He cryostat. The X-ray absorption spectra were collected as fluorescence excitation spectra[1] using a 13-element energy-resolving detector from Canberra Electronics,[2] and were referenced by I_0. Typical counts in the Mn fluorescence window for the central channel were 200 counts/sec at 6500 eV (below the Mn K-edge) and 1300 counts/sec at 6600 eV (above the Mn K-edge).

EXAFS spectra were collected at 3 eV/point from 6400 to 6540 eV with a collection time of 1 sec per point, 0.25 eV/point from 6540 to 6550 eV with a collection time of 1 sec per point, and at 1 eV/point from 6550 eV to 6576 eV with a collection time of 1 sec per point. The EXAFS region was collected with points evenly spaced every 0.05 $Å^{-1}$ in *k*-space from 2.05 $Å^{-1}$ to 12 $Å^{-1}$, with E_0 assigned as 6563 eV. The time of collection was weighted using a cubic function from a minimum of 1 sec per point at low *k* values to a maximum of 10 sec per point at high *k* values.

Collection of an energy-reference spectrum was achieved by placing a $KMnO_4$ sample between two N_2-filled ion chambers, I_1 and I_2, which were positioned behind the PS II sample, and collecting a $KMnO_4$ absorption spectrum concurrently with PS II data collection. The narrow pre-edge line (FWHM ≤ 1.7 eV) at 6543.3 eV was subsequently used for energy calibration.[3]

Data reduction was performed by removal of a linear pre-edge background, followed by normalization of the edge jump by fitting a quadratic polynomial to the EXAFS region (6570 – 7100 eV) and assigning the intensity of the extrapolated polynomial to 1.0 at 6563 eV. The resulting spectra were then divided by the tabulated free-atom absorption values from McMaster et al.[4] Residual background removal was obtained by fitting a quadratic polynomial to the region between 6750 eV and 7100 eV and subtracting the resulting polynomial from the entire EXAFS spectrum. Conversion of EXAFS spectra into *k*-space was performed using the formula in Eq. S1:

$$k\ (Å^{-1}) = \sqrt{\frac{2m_e}{\hbar^2}(E - E_0)} \qquad \text{Eq. S1}$$

where *k* is the photoelectron momentum ($Å^{-1}$), also referred to as the photoelectron wavevector; m_e is the electron mass; $\hbar = h/2\pi$, where *h* is Planck's constant, and E_0 is the threshold energy

for photoelectron production. Although the value of E_0 was fixed at 6563 eV for the *k*-space conversion, subsequent curve-fitting using the EXAFS equation (Eq. 1 in the main text) treated E_0 as a variable parameter. The *k*-space spectra were then multiplied by k^3 to generate k^3-weighted EXAFS spectra; this largely offsets the damping of the EXAFS oscillations seen in the non-k^3-weighted *k*-space spectra. As shown in the EXAFS equation, this is mainly due to the $1/(kR^2)$ amplitude dependence of the EXAFS oscillations and the fact that the *ab initio* amplitude function $f_{eff_j}(\pi, k, R_j)$ is roughly $1/k^2$ dependent.[5] Because low-frequency background contributions were apparent in the Fourier transforms of the uncorrected spectra as peaks at $R' < 1$ Å, further background removal of a 5-domain spline in k^3-space was necessary.

To simplify the curve-fitting procedure, the individual Fourier peaks I, II, and III were isolated and fit separately by applying a Hamming window to the first and last 15 % of the chosen range, leaving the middle 70 % untouched. In addition, the Fourier peaks were isolated and fit in pairs (I + II, II + III) to minimize possible distortions from isolating closely spaced Fourier peaks separately. However, as mentioned by Latimer et al.[6], there is a tradeoff in doing this, because the fits to pairs of Fourier peaks are dominated by the contribution from the larger peak, making it difficult to reliably extract information from the smaller Fourier peak. This is particularly relevant for fits to peaks II and III.

Comparison of deconvolution methods for S_0-state EXAFS spectra

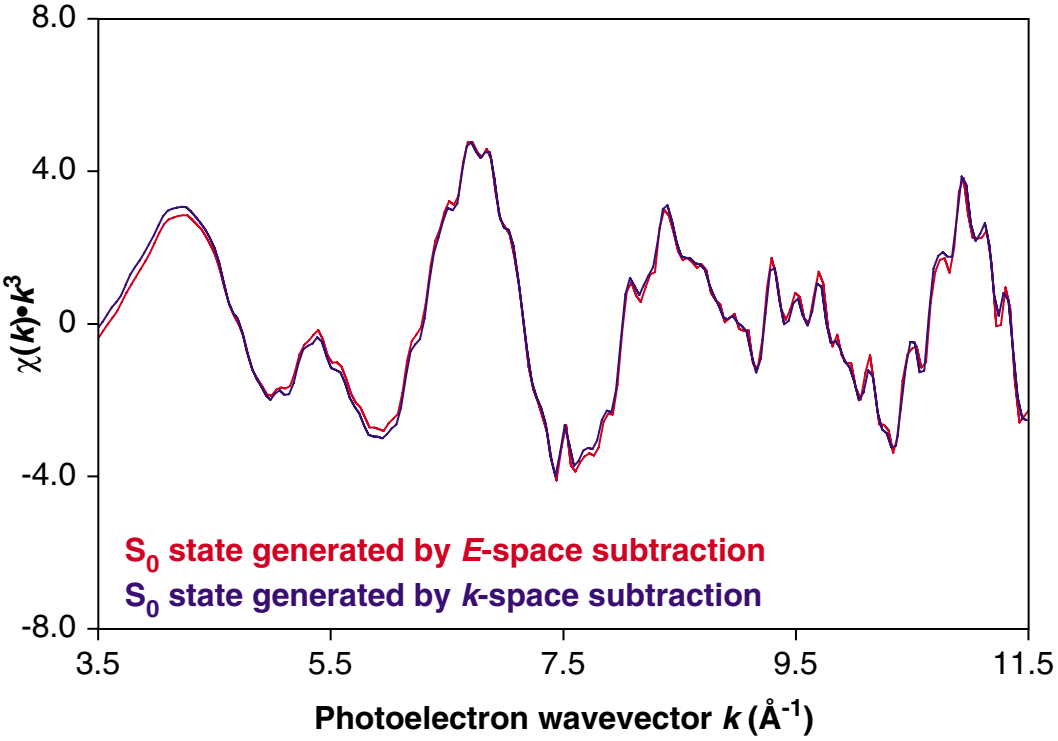

Figure S1: Mn K-edge EXAFS spectra of the S_0 state generated by deconvolution in *E*-space (red) and in k^3-space (blue). The data analysis of the S_0 state reported in this paper is based on the deconvolution in *E*-space.

Deconvolution of the 3F EXAFS spectra into pure S_0-state EXAFS spectra can be performed in two ways. The S_1-state spectrum can be subtracted from the 3F spectrum after normalization in *E*-space and before conversion into k^3-space. Alternatively, the S_1-state spectrum can be subtracted from the 3F spectrum after both spectra have been converted into k^3-space using the methods detailed in the Materials and Methods section. Although the former method is preferred because only one round of background removal is performed to the S_0-state spectrum, the latter method is often used because the signal-to-noise ratio is often insufficient for subtraction before conversion into k^3-space. For the results presented in this paper, the high signal-to-noise ratio permitted the deconvolutions to be performed before conversion into

k^3-space. However, to ensure that this did not affect the data analysis, the deconvolution was performed after the conversion into k^3-space. Figure S1 and Figure S2 show that the resulting spectra are virtually identical. Furthermore, the curve-fitting results to the Fourier isolates generated from both of the S_0-state spectra shown in Figure S2 show virtually identical results for the two deconvolution methods (data not shown); thus, the choice of deconvolution method did not affect the data analysis.

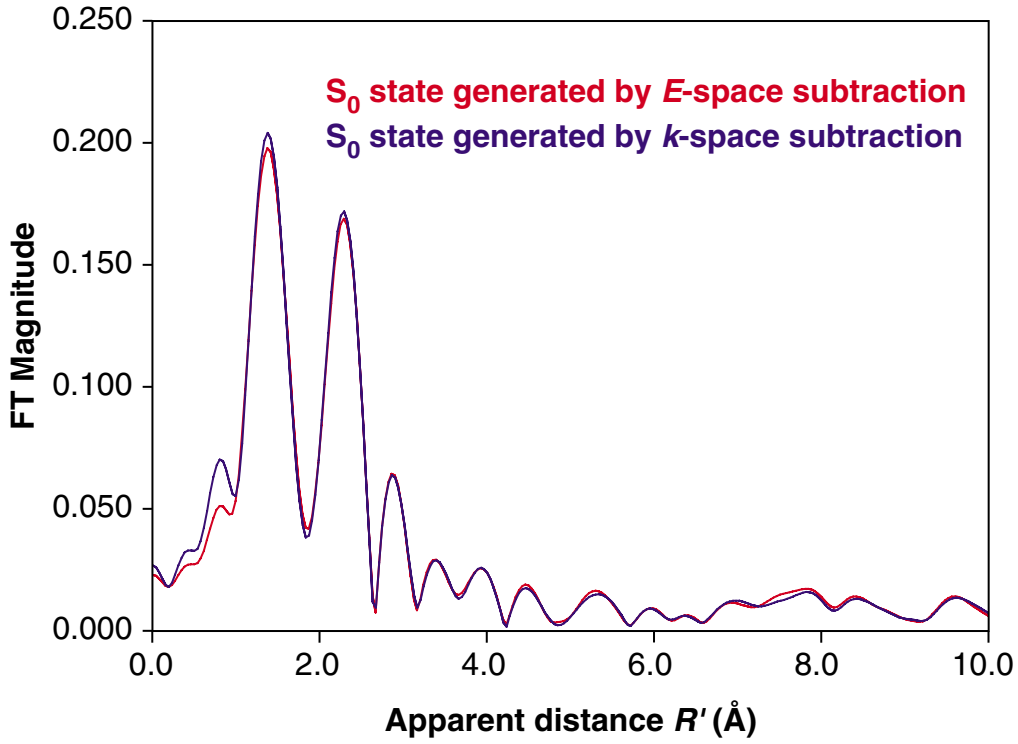

Figure S2: Fourier transforms of Mn K-edge EXAFS spectra from Figure S1 of the S_0 state generated by deconvolution in *E*-space (red) and in k^3-space (blue). The data analysis of the S_0 state reported in this paper is based on the deconvolution in *E*-space.

Consideration of possible radiation damage effects

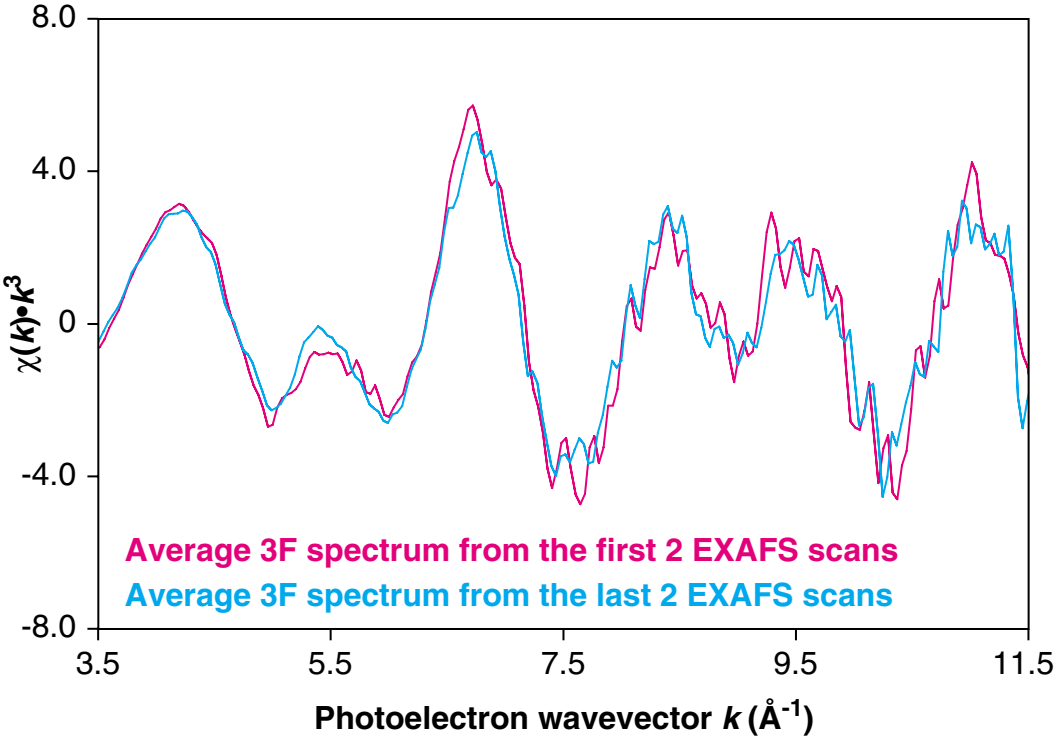

Figure S3: Average k^3-weighted EXAFS spectra from 3F samples showing the effects of radiation damage. The average spectrum from the first 2 EXAFS scans on each region of the sample is shown in pink, and the average spectrum from the last 2 EXAFS scans on each region of the sample is shown in light blue. A total of 24 scans were averaged for each spectrum.

As described in the Materials and Methods section, the experimental protocol of the S_0-state EXAFS experiments was designed to minimize and monitor radiation damage by collecting only 8 EXAFS scans on each separate region of the sample. To evaluate the effects of possible radiation damage on the EXAFS spectra, the average k^3-space spectrum of the first 2 EXAFS scans collected on each sample region of the 3F samples was compared to the average k^3-space spectrum of the last 2 EXAFS scans collected on each sample region. A total of 24 scans were averaged for each spectrum. Figure S3 shows that there is very little change between the two k^3-space spectra from the 3F samples. Furthermore, the curve-fitting results from both of

the spectra shown in Figure S3 are virtually identical (data not shown). Therefore, radiation damage effects are assumed to be minimal for the EXAFS spectra presented in this paper.

Reproducibility of EXAFS spectra

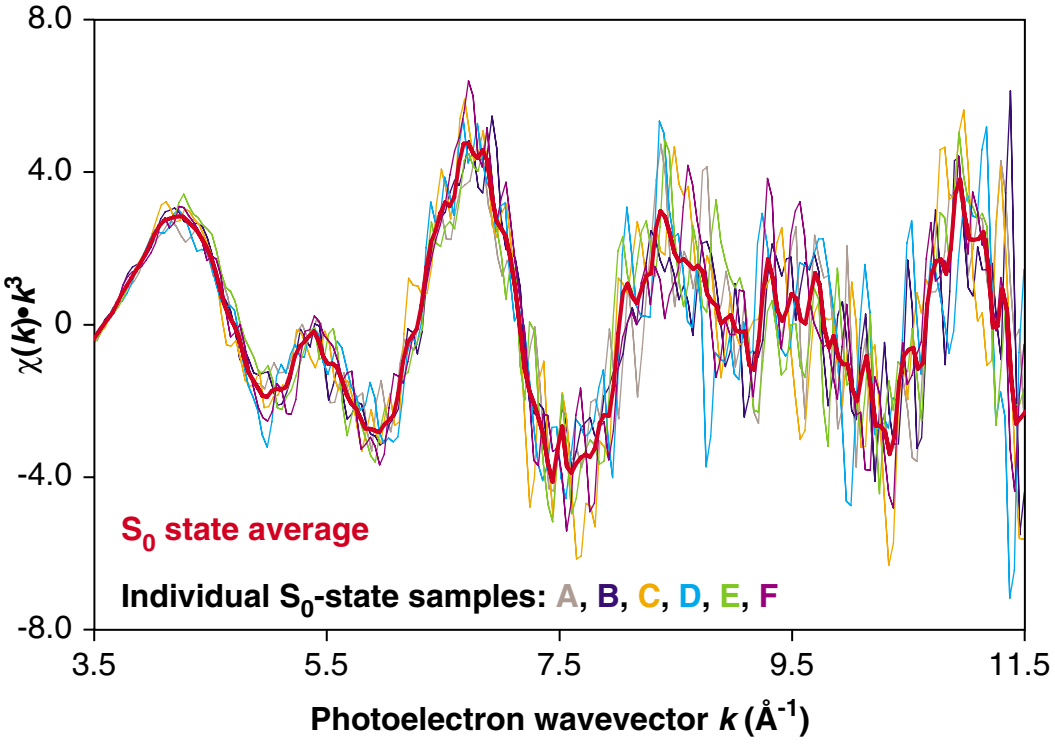

Each of the six 3F samples that were used to generate the average spectrum shown in

Figure S4: Mn K-edge EXAFS spectra of the S_0 state from six separate three-flash samples. Each three-flash spectrum was individually deconvoluted as described in Figure 3 to generate the six pure S_0-state spectra shown above. The S_0-state spectrum from Figure 3 is shown as a red line for comparison.

Figure 3 in the main text was deconvoluted separately using the average S_1-state EXAFS spectrum to generate six independent S_0-state EXAFS spectra; the results are shown in Figure S4. This shows that the loss of resolution of the EXAFS oscillations that is seen in the average spectrum is also seen in the spectra from the six individual samples.

The Fourier isolates from Peak II from each individual S_0-state data set are shown in Figure S5. These Fourier isolates show that the trends seen in the Fourier isolates generated from the Fourier transform of the average S_0-state spectrum are also seen the Fourier isolates generated from each individual sample. Specifically, the differences in the amplitude envelope of the S_0 and S_1-state Peak II Fourier isolates shown in Figure 6 that was interpreted as possible distance heterogeneity are also seen in the individual sample spectra shown in Figure S5. Thus, even before the curve-fitting procedures are applied, the consistency mentioned above greatly increases confidence in the conclusions.

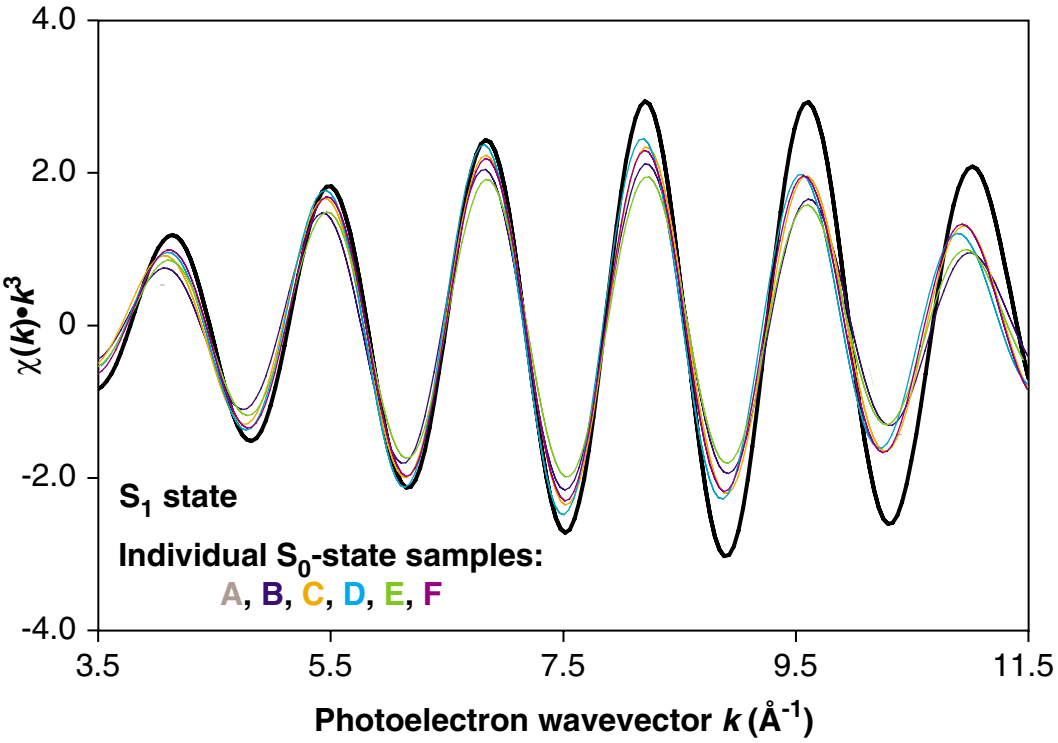

Figure S5: Fourier isolates from Peak II of the Fourier transforms generated from each of the six individual S_0-state spectra shown in Figure S4. The average S_1-state spectrum is shown in black. The difference in the amplitude envelope of the EXAFS oscillations between the two S-states is evident, and can be explained by the presence of two different Mn–Mn distances in the S_0 state with a small (< 0.2 Å) separation in distance.

Curve-fitting results from Peaks I+II and II+III

Table S1: Two- and three-shell simulations of Fourier peaks I and II from the S_0-state and S_1-state samples.

Fit #	sample	shell	R (Å)	N	σ^2 (Å^2)	ΔE_0 [b]	Φ (x 10^3)	ε^2 (x 10^5)
1	S_0 Grand Add	Mn–O	1.86	2.5[c]	0.005	-20	0.61	0.60
		Mn–Mn	2.72	1.24	0.005			
2	S_0 Grand Add	Mn–O	1.86	2.5[c]	0.005	-20	0.57	0.56
		Mn–Mn	2.67	0.65[d]	0.002[c]			
		Mn–Mn	2.78		0.002[c]			
3	S_0 Grand Add	Mn–O	1.87	2.5[c]	0.005	-18	0.51	0.50
		Mn–Mn	2.71	1.04[e]	0.002[c]			
		Mn–Mn	2.84	0.52[e]	0.002[c]			
4	S_1	Mn–O	1.84	2.5[c]	0.005	-20	1.26	1.02
		Mn–Mn	2.72	1.23	0.002			
5	S_1	Mn–O	1.84	2.5[c]	0.005	-20	1.25	1.02
		Mn–Mn	2.70	0.62[d]	0.002[c]			
		Mn–Mn	2.74		0.002[c]			
6	S_1	Mn–O	1.86	2.5[c]	0.005	-20	1.24	1.01
		Mn–Mn	2.69	1.01[e]	0.002[c]			
		Mn–Mn	2.78	0.51[e]	0.002[c]			

[a]fit parameters and quality-of-fit parameters are described in Materials and Methods; [b]ΔE_0 was constrained to be equal for all shells within a fit; [c]parameter fixed in fit; [d]the Mn–Mn N_1:N_2 ratio was fixed to 1:1 for this fit; [e]the Mn–Mn N_1:N_2 ratio was fixed to 2:1 for this fit

As mentioned in the Results section, the effects of possible Fourier isolation artifacts to the curve-fitting results was examined by isolating and fitting the Fourier peaks as pairs (Peaks I+II and Peaks II+III). As shown in Table S1 and Table S2, these results are essentially identical to those shown in the main text for the S_1-state and S_0 Grand Add samples. This was also true for pairwise fits for each of the individual S_0-state spectra S_0A through S_0F (data not shown). Thus, the effects of the Fourier isolation procedure are found to be negligible for the fits presented in the main text.

Table S2: Two- and three-shell simulations of Fourier peaks II and III.

Fit #	sample	shell	R (Å)	N	σ^2 (Å^2)	ΔE_0[b]	Φ (x 10^3)	ε^2 (x 10^5)
1	S_0 Grand Add	Mn–Mn	2.73	1.14	0.004	-18	0.25	0.32
		Mn–Mn	3.28	0.5[c]	0.005			
2	S_0 Grand Add	Mn–Mn	2.69	0.58[d]	0.002[c]	-18	0.24	0.31
		Mn–Mn	2.77	0.58[d]	0.002[c]			
		Mn–Mn	3.28	0.5[c]	0.005			
3	S_0 Grand Add	Mn–Mn	2.73	1.08[e]	0.002[c]	-14	0.20	0.27
		Mn–Mn	2.87	0.54[e]	0.002[c]			
		Mn–Mn	3.33	0.5[c]	0.004			
4	S_0 Grand Add	Mn–Mn	2.73	1.13	0.004	-17	0.24	0.32
		Mn–Mn	3.27	0.5[c]	0.002[c]			
		Mn–Ca	3.46	0.25[c]	0.002[c]			
5	S_0 Grand Add	Mn–Mn	2.70	0.58[d]	0.002[c]	-17	0.23	0.31
		Mn–Mn	2.78	0.58[d]	0.002[c]			
		Mn–Mn	3.27	0.5[c]	0.002[c]			
		Mn–Ca	3.45	0.25[c]	0.002[c]			
6	S_0 Grand Add	Mn–Mn	2.72	0.93[e]	0.002[c]	-15	0.21	0.28
		Mn–Mn	2.84	0.47[e]	0.002[c]			
		Mn–Mn	3.30	0.5[c]	0.002[c]			
		Mn–Ca	3.49	0.25[c]	0.002[c]			
7	S_1	Mn–Mn	2.72	1.05	0.001	-19	0.48	0.47
		Mn–Mn	3.23	0.5[c]	0.005			
8	S_1	Mn–Mn	2.73	0.61[d]	0.002[c]	-18	0.55	0.46
		Mn–Mn	2.73	0.61[d]	0.002[c]			
		Mn–Mn	3.26	0.5[c]	0.002[c]			
9	S_1	Mn–Mn	2.73	0.82[e]	0.002[c]	-18	0.55	0.46
		Mn–Mn	2.73	0.41[e]	0.002[c]			
		Mn–Mn	3.26	0.5[c]	0.002[c]			
10	S_1	Mn–Mn	2.73	1.23	0.002[f]	-17	0.46	0.39
		Mn–Mn	3.24	0.5[c]	0.002[c]			
		Mn–Ca	3.43	0.25[c]	0.002[c]			
11	S_1	Mn–Mn	2.73	0.61[d]	0.002[c]	-17	0.46	0.45
		Mn–Mn	2.73	0.61[d]	0.002[c]			
		Mn–Mn	3.24	0.5[c]	0.002[c]			
		Mn–Ca	3.43	0.25[c]	0.002[c]			
12	S_1	Mn–Mn	2.73	0.82[e]	0.002[c]	-17	0.46	0.45
		Mn–Mn	2.73	0.41[e]	0.002[c]			
		Mn–Mn	3.24	0.5[c]	0.002[c]			
		Mn–Ca	3.43	0.25[c]	0.002[c]			

[a]fit parameters and quality-of-fit parameters are described in Materials and Methods; [b]ΔE_0 was constrained to be equal for all shells within a fit; [c]parameter fixed in fit; [d]the Mn–Mn N_1:N_2 ratio was fixed to 1:1 for this fit; [e]the Mn–Mn N_1:N_2 ratio was fixed to 2:1 for this fit; [f]if the Debye-Waller parameter for this fit was not fixed, it went to a chemically unreasonable value of 0 Å^2

References

(1) Jaklevic, J.; Kirby, J. A.; Klein, M. P.; Robertson, A. S.; Brown, G. S.; Eisenberger, P. *Solid State Commun.* **1977**, *23*, 679-682.

(2) Cramer, S. P.; Tench, O.; Yocum, M.; George, G. N. *Nucl. Instrum. Methods Phys. Res., Sect. A* **1988**, *A266*, 586-591.

(3) Goodin, D. B.; Falk, K.-E.; Wydrzynski, T.; Klein, M. P. "SSRL Activity Report," Stanford Synchrotron Radiation Laboratory, 1979.

(4) McMaster, W. H.; Del Grande, N. K.; Mallett, J. H.; Hubbell, J. H. "Compilation of X-ray cross sections," Lawrence Radiation Laboratory, 1969.

(5) Powers, L. *Biochim. Biophys. Acta* **1982**, *683*, 1-38.

(6) Latimer, M. J.; DeRose, V. J.; Mukerji, I.; Yachandra, V. K.; Sauer, K.; Klein, M. P. *Biochemistry* **1995**, *34*, 10898-10909.